



HAL
open science

Structural and optical changes in silica-based optical fibers exposed to high neutron and gamma fluences

A. Morana, G. Cheymol, I. Reghioua, A. Boukenter, M.L. Schlegel, A. Gusarov, E. Marin, Y. Ouerdane, C. Destouches, S. Girard

► To cite this version:

A. Morana, G. Cheymol, I. Reghioua, A. Boukenter, M.L. Schlegel, et al.. Structural and optical changes in silica-based optical fibers exposed to high neutron and gamma fluences. *Journal of Non-Crystalline Solids*, 2021, 574, pp.121150. 10.1016/j.jnoncrysol.2021.121150 . ujm-03466352

HAL Id: ujm-03466352

<https://ujm.hal.science/ujm-03466352>

Submitted on 16 Oct 2023

HAL is a multi-disciplinary open access archive for the deposit and dissemination of scientific research documents, whether they are published or not. The documents may come from teaching and research institutions in France or abroad, or from public or private research centers.

L'archive ouverte pluridisciplinaire **HAL**, est destinée au dépôt et à la diffusion de documents scientifiques de niveau recherche, publiés ou non, émanant des établissements d'enseignement et de recherche français ou étrangers, des laboratoires publics ou privés.



Distributed under a Creative Commons Attribution - NonCommercial 4.0 International License

Structural and optical changes in silica-based optical fibers exposed to high neutron and gamma fluences

A. Morana,^{1,*} G. Cheymol,² I. Reghioua¹, A. Boukenter,¹ M.L. Schlegel,²
A. Gusarov,³ E. Marin,¹ Y. Ouerdane,¹ C. Destouches,⁴ and S. Girard¹

¹Univ Lyon, UJM, CNRS, IOGS, Laboratoire Hubert Curien, UMR 5516, 18 rue Prof. B. Lauras, Saint-Etienne, F-42000, France

²Université Paris-Saclay, CEA, Service d'Études Analytiques et de Réactivité des Surfaces, 91191, Gif-sur-Yvette, France

³SCK•CEN—Belgian Nuclear Research Center, Boeretang 200 2400 Mol, Belgium

⁴CEA, DEN, DER, Instrumentation Sensors and Dosimetry Laboratory Cadarache, Saint-Paul-Lez-Durance, F-13108, France

* adriana.morana@univ-st-etienne.fr

ABSTRACT

The optical fiber (OF) silica glass compaction is the least studied effect induced by radiation, since it takes place at very high fluences, mainly in mixed environments combining γ -rays and neutrons. Although the radiation-induced structural reorganization has already been investigated in bulk materials, OFs are a more complex case study, due to its inhomogeneous nature and internal stress distribution. We hereby investigate the structural changes induced in a pure-silica core OF by fast neutron fluence of up to 5×10^{19} n/cm² and total γ -dose of ~ 4 GGy(SiO₂), through micro-Raman spectroscopy allowing us to study the radial distribution of several signatures. The structural changes induced by neutrons on this OF are weaker than those observed on bulk glass at similar fluences, in agreement with the lower observed compaction. The main cause is the higher irradiation temperature, even if a key role is played by the internal stress present in the fibers.

Keywords: silica, compaction, neutrons, Raman spectroscopy, optical fibers, radiation (6)

1 INTRODUCTION

Optical fiber (OF) technology has become more and more widespread in the world of data transfer and sensing, thanks to its multiple advantages, such as compact size, light weight, passive operation ability and easy multiplexing property. Among all the kinds of fibers, the ones based on amorphous silica glass (SiO₂) are today the most common, even for applications in harsh environments, like nuclear reactors or nuclear waste repositories. However, such environments are characterized by ionizing radiation, neutrons and/or high temperature, which can compromise the OF and optical fiber sensor (OFS) performances due to radiation-induced point defects and structural changes, particularly compaction [1]. Whereas numerous studies deal with the radiation-induced OF transmission degradation [1-2], only few focus on radiation-induced compaction (RIC) in OFs [3-4]. However, even if there is extensive literature on radiation effects on the amorphous silica glass structural modifications (see references of [5]), the high temperature drawing process undergone by the preform leads to fiber material with properties differing from the bulk glass, such as the internal stress distribution, the precursor site nature for the defect generation as well as a glass fictive temperature varying along the fiber transverse cross section diameter [6].

Concerning studies about SiO₂ glass RIC, the reported density variation ($\Delta\rho$) depends on the absorbed irradiation dose (D) according to the following power law:

$$\frac{\Delta\rho}{\rho} \propto D^k \quad (\text{Eq. 1})$$

where k depends on the irradiation nature; $k \sim 1$ for fast neutrons and $\sim 2/3$ for γ -rays [7]. However, at high doses, the relative density increase reaches a saturation at a maximum value

of ~3%, beyond which it can no longer increase [8]. This final dense material is known as metamict state and its structure is still made by SiO₄ tetrahedra having O-Si-O angles and Si-O distances similar to pristine silica values (109.5° and 1.62 Å, respectively), but with more acute inter-tetrahedral Si-O-Si angles. This is explained by the puckering of the 6-membered rings [9] while the three- and four-membered ring concentrations increase [10]. It was observed that this phase is independent from the irradiation nature or the material [9].

In a recent publication [11], Petrie *et al.* improved the model describing the compaction as a function of the neutron fluence by including the irradiation temperature. Moreover, by comparing their results with the ones already reported in literature, the authors stated that the higher the irradiation temperature, the lower the saturation value of compaction.

Concerning the OFs, the neutron-induced compaction was recently studied within a collaborative framework between the SCK-CEN in Belgium and the CEA in France, to develop a Fabry-Perot type elongation OFS [12]. Optical fiber samples were exposed in the SCK-CEN BR2 reactor to different fast neutron fluences and the linear compaction was estimated thanks to very precise sample length measurements [3-4]. From these irradiation tests, the authors observed a linear compaction of ~0.3% at the neutron fluence of ~5×10¹⁹ n/cm² (with an additional γ-ray dose of ~4 GGy) at a temperature of ~290°C [3], and of ~0.29% and ~0.57% after a neutron fluence of 1 and 3×10¹⁹ n/cm², respectively, (with the additional γ-ray dose of 0.5 and 1.5 GGy) at ~250°C [4].

In order to investigate the neutron-induced structural changes on OFs, samples of a multimode pure silica core optical fiber irradiated in the BR2 reactor at two neutron fluences, 3 and 5×10¹⁹ n/cm², at ~290°C were studied through confocal Raman spectroscopy and the results were compared with the large bibliography on bulk silica. A few luminescent defect results are also reported here to support the discussion.

2 MATERIALS AND METHODS

The fiber under test is a multimode step index from Ceramoptec with a N.A of 0.12. Its pure silica core has a 50 μm diameter, whereas its cladding is constituted by two rings: the first one of F-doped silica with a ~10 μm width, and the second one (~27.5 μm width) of pure silica.

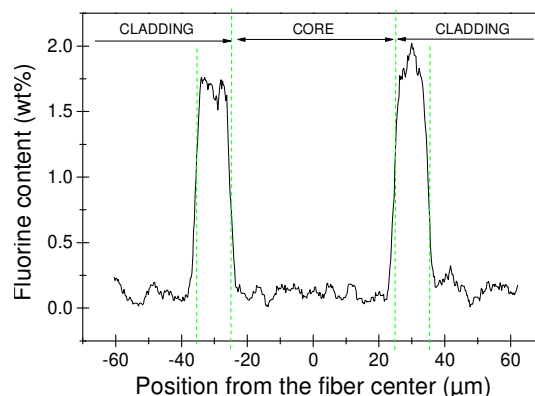


Fig. 1. EDX measurement of the F content. The dotted green lines mark the different parts of the fiber. (no color print)

Fig. 1 reports its fluorine content profile, as a function of the distance from the fiber center, recorded with a field emission scanning electron microscope (SEM) (JSM 7100f JEOL) equipped with energy dispersive X-ray (EDX) detector (X-Max 80, OXFORD) in the Nova Gorica University (Slovenia).

Such pure silica core OF was chosen as it presents a good RIA response, compared to other fiber types, under steady state irradiation at doses exceeding the MGy dose levels [13]. Two

uncoated samples were irradiated in the reflector channel of the SCK•CEN BR2 reactor during a 22 day cycle at $(290\pm 4)^\circ\text{C}$ with a fast neutron flux ($E > 1 \text{ MeV}$) of $\sim 2 \cdot 10^{13} \text{ n}/(\text{cm}^2 \cdot \text{s})$, up to two neutron fluences around 3 and $5 \cdot 10^{19} \text{ n}/\text{cm}^2$. The samples were pre-heated up to 290°C before the cycle start and cooled down after its end. The associated γ -dose-rate was $\sim 7.2 \text{ MGy}/\text{h}$, leading to an accumulated dose of 3.8 GGy. More details on the irradiation conditions are reported in ref. [3]. Another sample was not irradiated and kept as a reference. The length measurements were performed using a dedicated set-up, which allowed 0.01 - 0.03% accuracy [3]. Linear compactions of 0.27% and 0.24% were measured for the samples irradiated at the lower and higher fluences, respectively [3]. Under the hypothesis of an isotropic compaction, this corresponds to a $\sim 0.7\%$ density increase.

The induced structural changes were studied using Raman spectroscopy in different zones of the fiber-transverse-section with the integrated confocal microRaman Aramis system (from Horiba Jobin Yvon), equipped with a CCD camera, 3D-microtranslation stages and two laser probes: a He-Cd emitting at 325 nm or at 442 nm and a He-Ne at 633 nm, in the Hubert Curien Laboratory (Saint-Etienne, France).

Most spectra were excited at 325 nm and acquired through a $\times 40$ objective and a confocal $50 \mu\text{m}$ hole diameter, leading to a $3 \mu\text{m}$ spatial resolution at different points along two orthogonal fiber diameters. With the same confocal system, photoluminescence (PL) spectra were acquired under excitation at 325 nm, as a function of the position along the fiber transverse surface. Other Raman spectra were collected via a LabRam HR800 (Horiba Jobin Yvon) with an excitation wavelength of 785 nm, a $\times 50$ long-range objective and a $100 \mu\text{m}$ hole at CEA Saclay (France).

The experimental Raman spectra were reduced by the thermal population and the scattering absolute frequency dependence, as explained by Shimodaira *et al.* [14], and then normalized with respect to the area between 270 and 1350 cm^{-1} . At lower wavenumbers the signal is distorted by the notch-filter and at the higher ones by photoluminescence contributions. For each sample, the Raman spectra were recorded along two orthogonal diameters on the fiber-transverse-section, in order to have two spectra corresponding to a same distance from the fiber center. Thus, to the different parameters characterizing the Raman bands, such as center, width and area, as a function of the distance from the core center, were attributed the average and the standard deviation, as uncertainty, of the two values obtained on two corresponding points along the two diameters.

3 RESULTS

3.1 Raman spectroscopy

As an example, Fig. 2(a) reports the normalized Raman spectra recorded in the core center of the three samples, pristine or irradiated at the two neutron fluences.

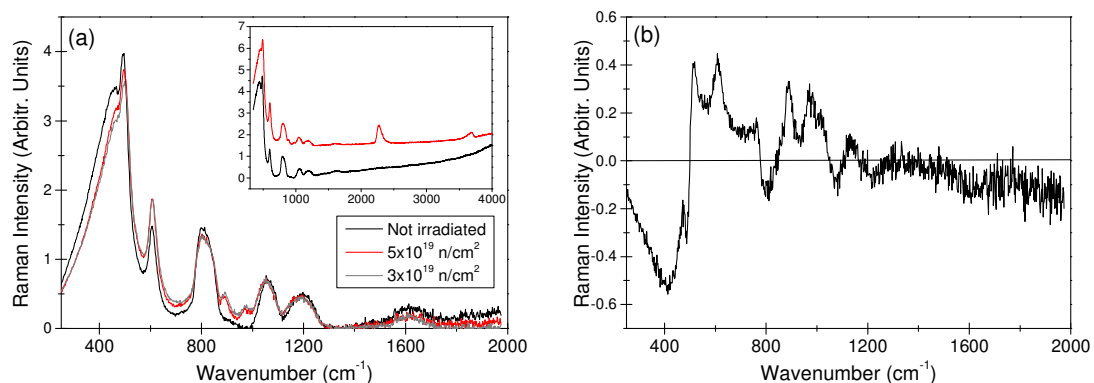


Fig. 2. (a) Reduced and normalized Raman spectra recorded in the fiber center for the three samples: non-irradiated (black line) and irradiated at two fluences of 3 and $5 \cdot 10^{19} \text{ n}/\text{cm}^2$ (grey and red lines, respectively). In the inset, extended spectra up to 4000 cm^{-1} (normalized

to the band at $\sim 800\text{ cm}^{-1}$ and to which an arbitrary constant has been added). (b) Difference between the Raman spectra acquired on the neutron irradiated sample at the highest fluence and on the pristine one. (no color print)

Fig. 2(b) shows the difference between the spectra acquired on the pristine sample and the one exposed at the highest neutron fluence, highlighting the neutron-induced structural changes.

From Fig. 2, it is clear that neutrons cause:

- a shift towards the higher wavenumbers and a narrowing of the R band, the main one at $\sim 440\text{ cm}^{-1}$, assigned to bridging oxygens symmetric stretching in n-membered $(\text{SiO})_n$ rings, where n vary from 5 to 10 with most of the rings having 6 size [15];
- an intensity increase (and consequently of the area) of the D_2 band around 606 cm^{-1} , associated with bridging oxygen breathing motion in three-membered rings [15];
- a slight change in the ω_3 band at $\sim 800\text{ cm}^{-1}$, which is associated with the TO/LO (Transverse or Longitudinal Optical) split bending modes [15];
- a new band appearance centered at $\sim 890\text{ cm}^{-1}$, whose origin is still in debate and will be discussed later in more depth;
- a shift towards lower wavenumbers of the ω_4 band components, peaking at ~ 1060 and $\sim 1200\text{ cm}^{-1}$, which are attributed to the asymmetric TO and LO stretching of bridging oxygens [15];
- the appearance of three bands, highlighted in the inset of Fig. 2(a), centered at:
 - o 967 cm^{-1} , related to Si-OH stretching [16],
 - o 2260 cm^{-1} , associated with Si-H stretching [17];
 - o 3680 cm^{-1} , attributed to SiO-H stretching [17].

No significant change can be observed directly from Fig. 2 on the D_1 band, which peaked at 495 cm^{-1} and is associated with bridging oxygen breathing motion in four-membered rings [15].

In order to quantitatively calculate the position shifts or area changes of the Raman bands, the Raman spectra were decomposed as a sum of Gaussian and/or Lorentzian curves. In particular, as shown in Fig. 3, the spectral region between 240 and 700 cm^{-1} was fitted with two Lorentzian functions, one for the D_1 band and the other for the D_2 , and three Gaussian curves, whose sum, as already shown by Shimodaira et al. [14], allows to simulate mathematically the R band asymmetry, due to the variety of the $(\text{SiO})_n$ rings, for the Raman spectra recorded on both the pristine and the irradiated samples, since on these latter the feature becomes narrower and cannot be described by two Gaussians.

The second Raman spectrum part between 750 and 1300 cm^{-1} was fitted with six Gaussian curves, as reported in Fig. 4: two components (peaking at ~ 800 and 840 cm^{-1}) to simulate the ω_3 band asymmetry, one for each of the two ω_4 band components and one for the Si-OH stretching band. Moreover, a sixth Gaussian peaking at $(890.7 \pm 1.1)\text{ cm}^{-1}$ with full width at half maximum (FWHM) of $(44 \pm 6)\text{ cm}^{-1}$ was necessary to approximate a new Raman feature absent in the pristine sample and whose origin is still currently open to research. Its area was constant at (0.038 ± 0.009) arbitrary units along the fiber diameter.

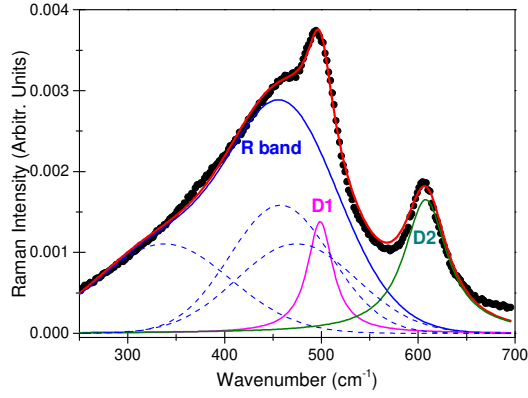


Fig. 3. Example of the fitting performed on the spectral region between 240 and 700 cm^{-1} acquired on the fiber center of the sample irradiated at the highest fluence: measured spectrum (dots) and fitted curve (lines). The red line is the overall curve, constituted by three Gaussian functions for the R band (blue dotted curves for the components and blue continuous curve for their sum) and two Lorentzian functions for the D₁ (pink continuous curve) and D₂ (green continuous curve) bands. (no color print)

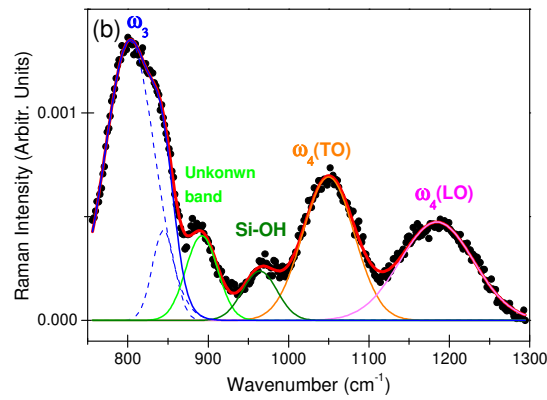


Fig. 4. Example of the fitting performed on the spectral region between 750 and 1300 cm^{-1} : measured spectrum (dots) and fitted curve (lines) for the spectrum acquired on the fiber center of the sample irradiated at the highest fluence. The red line is the overall curve constituted by six Gaussian functions: two for the ω_3 band at $\sim 800 \text{ cm}^{-1}$ (blue dotted curves for the components and blue continuous curve for their sum), one unknown about 890 cm^{-1} (light green curve), one at $\sim 965 \text{ cm}^{-1}$ attributed to the Si-OH vibration (dark green curve), one at 1060 and another at 1200 cm^{-1} , associated with the asymmetric stretching of bridging oxygens (orange and pink curves, respectively). (no color print)

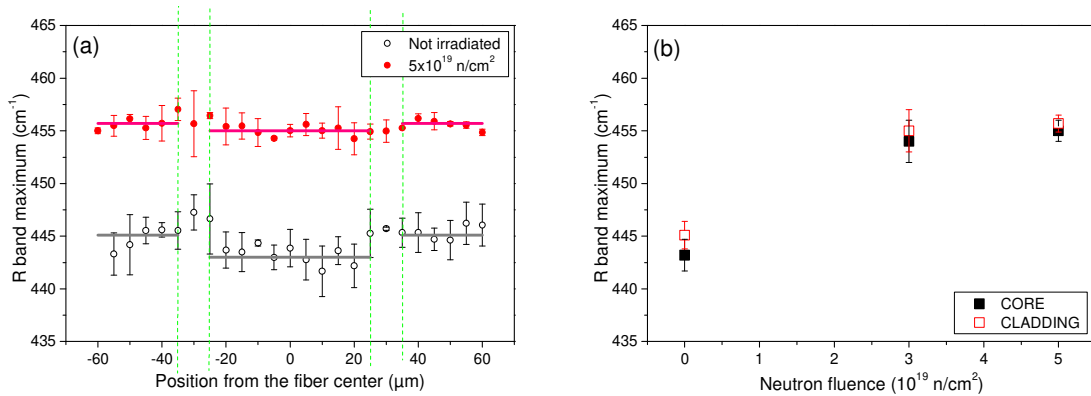


Fig. 5: (a) R band maximum as a function of the radial distance from the center along the fiber diameter, for the pristine sample (black empty circles) and the one irradiated at the highest fluence (red full circles). The grey and pink continuous lines represent the average of the R band position in the pure silica zones of the core and the cladding (except for the F-doped region, separated by dashed green lines), for the non-irradiated and irradiated samples, respectively. (b) Average of the R band maximum value, as a function of the neutron fluence, in the pure silica zones of core (black full squares) and cladding (red empty squares). (no color print)

Fig. 5(a) reports the position of R band maximum, determined as the maximum of the sum of the three Gaussian curves, as a function of the radial distance from the center for the fibers (pristine and irradiated at the highest neutron fluence). The R band position is constant along the fiber diameter with a slight difference (less than 2 cm^{-1}) between the pure silica core and

cladding zones. As highlighted in Fig. 5(b), where the values averaged on the two zones, core and cladding, are reported as a neutron fluence function, the R band shifts by about 12 cm^{-1} towards the higher wavenumbers for both neutron fluences.

The ω_3 band components, also, shift towards the higher wavenumbers of $\sim 10 \text{ cm}^{-1}$; however, it is difficult to isolate the two contributions effectively and, since no major information can be obtained from this band, we will not discuss more about it.

Concerning the D_1 and D_2 bands, approximated with two Lorentzian curves, one for each Raman feature (Fig. 3), their area values are displayed in Fig. 6 and 7(a), respectively, as a function of the radial distance from the fiber center, for the pristine sample and the one irradiated at the highest neutron fluence.

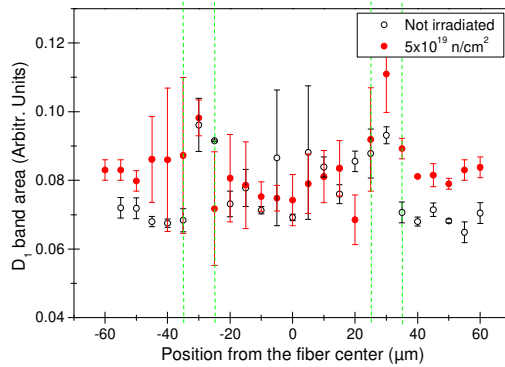


Fig. 6: D_1 band area as a function of the radial distance, for the pristine sample (black empty circles) and the one irradiated at the highest fluence (red full circles). (no color print)

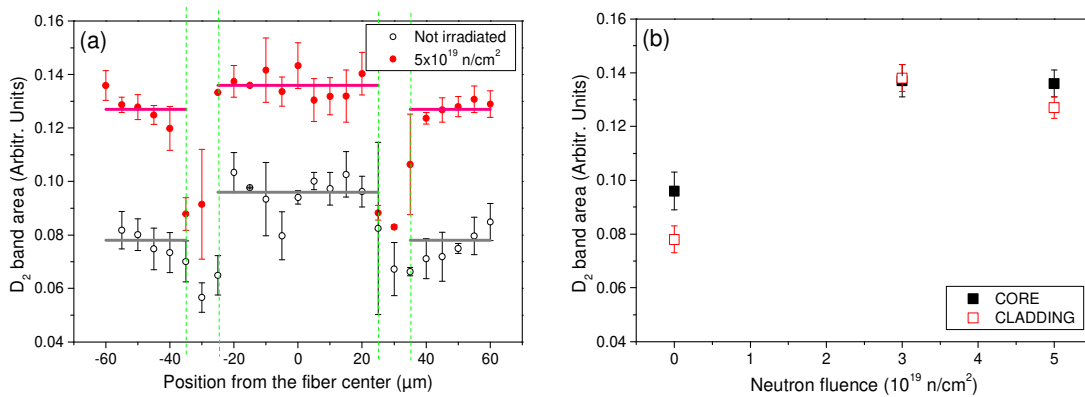


Fig. 7: (a) D_2 band area as a function of the radial distance, for the non-irradiated sample (black empty circles) and the one irradiated at the highest fluence (red full circles). The grey and pink continuous lines represent the average of the D_2 band area in the pure silica zones of the core and the cladding (except for the F-doped zone, separated by dashed green lines), for the pristine and the most irradiated samples, respectively. (b) Average of the D_2 band area value, as a function of the neutron fluence, in the pure silica zones of core (black full squares) and cladding (red empty squares). (no color print)

Independently of irradiation, the D_1 band area increases slightly with radial distance in the core and remains constant in the pure silica part of the cladding (within uncertainties). Moreover, no significant neutron-induced effect can be observed in the core, whereas the D_1 band area increases by $\sim 20\%$ with the neutron fluence in the cladding. However, it is worth noticing that the uncertainty associated with the D_1 band area is larger than for D_2 , due to overlapping between the D_1 and R bands.

The D_2 band area, instead, is constant in the core, whereas in the cladding it increases slightly with increased radial distance. By neglecting the variations of the D_2 band area in the pure silica zone of the cladding, Fig. 7(b) illustrates the values averaged on the two zones,

core and cladding, and highlights that the three-membered ring concentration tends to saturate, independently of its initial value.

Moreover, the spectral decomposition also allows highlighting a peak shift of 5 and 3 cm^{-1} towards higher wavenumbers of the D_1 and D_2 bands respectively, and a FWHM increase of a few cm^{-1} , as reported in Table I.

Fluence	D ₁ band		D ₂ band	
	Peak (cm^{-1})	FWHM (cm^{-1})	Peak (cm^{-1})	FWHM (cm^{-1})
0	493.6±1.3	29.16±0.02	604.8±1.4	42.63±0.02
3×10 ¹⁹ n/cm ²	498.3±1.3	32.26±0.02	607.9±1.6	52.882±0.014
5×10 ¹⁹ n/cm ²	498.6±0.3	33.09±0.02	607.3±0.6	48.38±0.02
Neutron induced shift	5	~4	3	>5

Table I. Peak position and FWHM of the D_1 and D_2 bands as a function of the neutron fluence.

Contrary to the other bands, the ω_4 band components at ~ 1060 and ~ 1200 cm^{-1} shift towards the lower wavenumbers of ~ 9 and ~ 14 cm^{-1} , respectively, as reported in Table II. However, no significant effect is observable in their area and FWHM (of ~ 70 and 110 cm^{-1} , respectively).

Fluence (10 ¹⁹ n/cm ²)	ω_4 band peaks position (cm^{-1})	
	TO component	LO component
0	(1059±2)	(1200±1)
3	(1050±1)	(1185±1)
5	(1051±3)	(1187±4)

Table II. Peak positions of the ω_4 band components as a function of the neutron fluence.

Finally, the band areas at 2260 and 3680 cm^{-1} were calculated from the extended Raman spectra after normalizing at 800 cm^{-1} and subtracting a linear baseline in the ranges from 2050 to 2750 cm^{-1} and from 3400 to 3850 cm^{-1} , respectively. Fig. 8 reports the values of these band areas as a function of the radial distance and highlights that the concentrations of SiH and SiOH bonds are higher in the cladding than in the core.

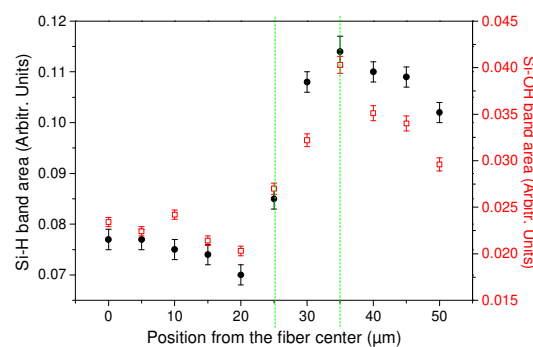


Fig. 8 Area of the Si-H (black full circles and left axis) and the SiO-H (red empty squares and right axis) bands as a function of the radial distance, for the sample irradiated at 5×10^{19} n/cm². (no color print)

By calculating the SiOH band area mean value along the entire fiber transverse surface and by comparing it with the area of the same band observed on a silica bulk sample having a known OH concentration, the OH concentration was estimated at ~ 4000 ppm and corresponds to 10^{20} OH groups/cm³. The presence of SiOH or SiH bonds is due to the radiation-induced defect interaction, such as NBOH and E' centers, respectively, with H⁺ ions [18]. The latter could not originate from either the fiber coating, which was removed before irradiation, nor

from water molecules because the samples were inside tight capsules. However, part of hydrogen atoms could originate from the air inside the capsules, and another part could have been created by the neutron interaction with the capsule material (stainless steel AISI 304).

3.2 Photoluminescence spectroscopy

Figure 9(a) reports the photoluminescence spectra emitted from the three sample fiber cores. The pristine sample presents two weak signals, one centered at 2.4 eV, whose origin is still debated [19], and the other at 1.9 eV, associated with Non-Bridging Oxygen Hole Centers (NBOHCs) [20]. However, the PL spectra of the irradiated fibers show an intense signal that is constituted by two Gaussian bands (Fig. 9(b)): an intense one centered at ~ 2.27 eV (546 nm) with FWHM of 0.36 eV and another centered at ~ 2.01 eV (~ 617 nm) with FWHM of 0.31 eV at lower intensity.

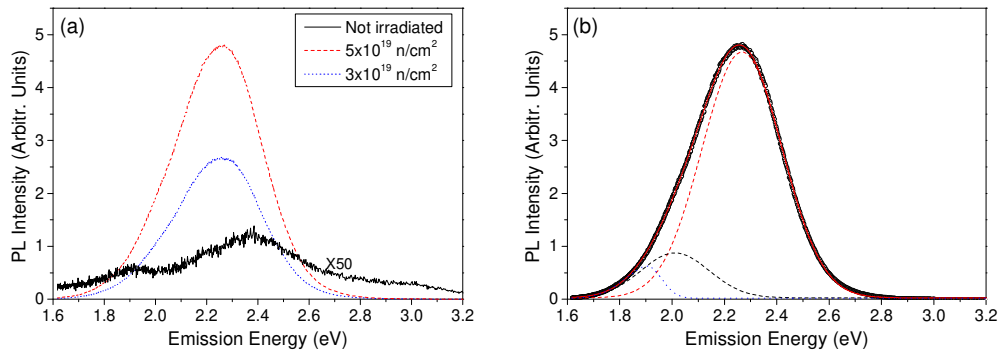


Fig. 9. (a) Photoluminescence spectra emitted under excitation at 325 nm from the core center of the samples: non-irradiated (black curve) and irradiated at two fluences of 3 and 5×10^{19} n/cm² (blue and red lines, respectively). (b) Decomposition of the PL spectra acquired in the core center of the fiber irradiated at the highest fluence with two Gaussian curves: measured spectrum (dots), fitted curves (two Gaussians in dashed red lines and the overall curve in continuous red line); the shape of the typical NBOHC PL band at 1.9 eV (dotted blue line) is reported as comparison. (no color print)

No defect structure is today associated with these bands. However, a band centered at 2.28 eV with FWHM of 0.47 eV has already been observed in neutron-irradiated fibers [19] and silica bulks [21] and even on silica bulk irradiated by femtosecond laser [22]. The other band is centered at 2 eV but it does not seem to be related to NBOHCs; indeed, the band is wider, centered at higher energy and it does not present the typical asymmetrical shape of the NBOHC PL [20]. The PL distribution along the fiber diameter of the two irradiated samples, displayed in Fig. 10, highlights that the defects originating the 2.3 eV PL are mainly induced in the fiber core rather than in the cladding, independently of the neutron fluence.

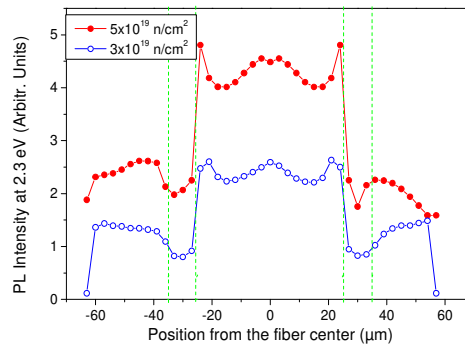


Fig. 10. Profile of the PL band at 2.30 eV (540 nm) along the fiber diameter of the samples irradiated at the two neutron fluences: 3 and 5×10^{19} n/cm² (blue empty circles and red full circles, respectively). (no color print)

4 DISCUSSION

The Raman spectra of the irradiated fibers feature the same trends as those observed on silica bulk glasses by Bates *et al.* [10] and previously by Stolen *et al.* [23], who studied the correlation between the density variation and the changes induced on Raman spectra of silica glasses by neutron irradiation up to $\sim 10^{20}$ n/cm². In fact, the R, D₁ and D₂ bands shift towards the higher wavenumbers, whereas the TO and LO components of the ω_4 band shift towards the lower wavenumbers. Table III compares the estimates of the Raman band shifts observed on two silica bulks irradiated by neutrons with energy (E) greater than 0.18 MeV at 5×10^{19} n/cm² and at 2×10^{20} n/cm² by Bates *et al.* [10] and on our fibers irradiated at a fluence of 5×10^{19} n/cm² with E > 1 MeV, which corresponds to $\sim 7 \times 10^{19}$ n/cm² with E > 0.18 MeV. It is worth noticing that:

- the neutron energy distributions in the two reactors, used in ref. [10] and in our study, are not identical, and the interaction probability depends on the neutron energy;
- the irradiation temperature was 60°C for ref. [8,10] and 290°C for our samples.

Consequently, part of the differences could be related to the testing conditions.

Fluence (n/cm ²)	Bates <i>et al.</i> [10] – Silica Bulk		Our data – Optical Fibers
	5×10^{19} (E>0.18 MeV)	2×10^{20} (E>0.18 MeV)	5×10^{19} (E>1 MeV) $\Rightarrow \sim 7 \times 10^{19}$ (E>0.18 MeV)
Irradiation Temperature (°C)	55		290
Compaction	2.4%	2.2%	0.7% [10]
R band shift (cm ⁻¹)	15		12
D ₁ band shift (cm ⁻¹)	10		5
D ₂ band shift (cm ⁻¹)	4		3
TO ω_4 band shift (cm ⁻¹)	N.A.	-22	-9
LO ω_4 band shift (cm ⁻¹)	N.A.	-25	-14

Table III. Comparison between the Raman bands shift observed by Bates *et al.* [10] on silica bulk and in this paper on silica fibers (N.A. means not available).

The volumetric compaction induced on the optical fibers investigated here, as calculated from direct length measurements [3] under the hypothesis of isotropic compaction, is $\sim 0.7\%$, which is lower than the one observed on the silica bulk, $\sim 2.3\%$, at similar neutron fluences [8]. According to the standard picture [24], fast neutron ballistic collisions with host atoms lead to a cascade of displaced atoms. Then, the cascade becomes a heat spike, a region that has a lower density in the middle and higher density on the border. After about 1 ps, the atoms in the spike reach an equilibrium-like (Maxwell-Boltzmann) distribution of kinetic energies, i.e. they behave like a thermodynamic system with a “temperature” of the order of $\sim 10^4$ K. The cooling down of the heat spike can be considered as a rapid (\sim ps time scales) liquid-solid transition. Since the cooling occurs very quickly, the atomic order cannot be restored and a number of liquid-relevant configurations remain frozen. A characteristic feature of such transition is its non-exponential stretched kinetics, with the relaxation rate decreasing when approaching the glass transition temperature (T_g) [25]. Therefore, even if the irradiation temperature is significantly below T_g , it may influence the concentration of displaced atoms, i.e. the final state density. The results reported in [8,10] were obtained on samples irradiated at temperature below 60°C. In our case the samples were at a constant temperature of 290°C

throughout the irradiation exposure. It is thus expected that a more advanced relaxation stage with a smaller density deviation could be reached, as already reported by Petrie *et al.* [11]. The smaller compaction seems reflected in smaller band shifts. However, it is worth also noticing that the band centers have not been determined in the same way in this study and in ref. [10], because the very intense luminescence observed in the Raman spectrum acquired in the irradiated silica bulk by Bates *et al.* prevents good background removal and normalization and could also influence the Raman band center determination.

An important parameter to describe the glass structure is the fictive temperature (T_f), defined as the one at which the liquid structure is frozen through the glass transition [26]. This temperature can be determined from Fourier Transform InfraRed or Raman spectra, in particular from the maximum of the main band or from the intensities and peak positions of the D_1 and D_2 bands [26]. A calibration curve linking the R band frequency (ω_1) with T_f was reported by Martinet *et al.* for homogenous pure silica samples:

$$\omega_1 = a \cdot T_f + b \quad (\text{Eq. 2})$$

where a is equal to $0.02 \text{ cm}^{-1}/^\circ\text{C}$ and b is $(419.5 \pm 0.5) \text{ cm}^{-1}$ [6]. However, these coefficients can vary with the presence of impurities, as OH and Cl, which enhance the structural relaxation [27]. Consequently, under the hypothesis that the relationship of Eq. 2 remains valid, we can deduce that T_f varies from $(1230 \pm 70)^\circ\text{C}$ to $(1790 \pm 50)^\circ\text{C}$ at the highest neutron fluence, regardless of the probed radial position in the core or cladding. This fictive temperature increase of $(560 \pm 100)^\circ\text{C}$ is larger than the one observed by Léon *et al.* [28] on silica bulk samples, that were irradiated at lower neutron fluences, up to 10^{18} n/cm^2 , but a lower temperature, 50°C .

A calibration curve also exists for the D_2 band area [6]; however, this cannot be easily applied, due to its strong dependence on the used spectrum normalization technique.

Because of the linear dependence between the silica density and the fictive temperature [29], the spatial distribution of this latter allows us to state that the density increase is uniform (within the error associated with the T_f measurements) along the fiber diameter, independently of the distance from the fiber center.

More information about the structural changes induced by neutron irradiation and giving rise to the compaction can be extracted by other Raman features. For example, the central force model by Sen and Thorpe [30] allows us to evaluate the mean inter-tetrahedral Si-O-Si angle (θ) for large rings from the R band mean frequency (ω_1) through the relation:

$$\omega_1^2 = \frac{2\alpha}{m_O} \left[\cos\left(\frac{\theta}{2}\right) \right]^2 \quad (\text{Eq. 3})$$

where m_O is the oxygen atomic mass and α is the Si-O stretching central force constant, that is $\sim 545 \text{ N/m}$ [31]. By assuming the force constant unchanged under densification, the angle θ can be calculated from the comparison with reference data (indicated with the subscript 0) [31]:

$$\cos\left(\frac{\theta}{2}\right) = \cos\left(\frac{\theta_0}{2}\right) \cdot \frac{\omega_1}{(\omega_1)_0} \quad (\text{Eq. 4})$$

For example, it is known that the Si-O-Si angle of 144° corresponds to the average R band position at 441 cm^{-1} [6].

Since the R band mean wavenumber increases from 412.5 cm^{-1} to 423.1 cm^{-1} , we obtain a decrease of $\sim 1^\circ$ for the inter-tetrahedral Si-O-Si angle in both core and cladding, which is a

slightly less than the angle reduction of $\sim 1.5^\circ\text{C}$ observed by Léon *et al.* on their silica bulk samples irradiated up to 10^{18} n/cm² at 50°C [28].

As the mean Si-O-Si angle associated with the larger rings decreases, the one related to the small rings does too [32]. The breathing modes are not pure bending vibrations and a precise model to describe them does not exist. However, the simple model by Sen and Thorpe [30], reported in Eq. 3, can also be considered valid for the small rings, but with different force constants. Consequently, by using the comparison method of Eq. 4 with the reference data of Table IV and the results reported in Table I, the inter-tetrahedral angle of the four-membered rings decreases by $\sim 0.44^\circ$ (from 138.02° to 137.57°), whereas the one associated with the three-membered rings is reduced by $\sim 0.23^\circ$ (from 127.62 to 127.38°). It is worth noticing that the variation induced on the fourfold rings is slightly larger than on the threefold ones, as already observed for densification through compression [32]. Moreover, both small rings seem to be affected more by the neutron-induced densification than by the compression, indeed for 20% compression-induced densification on silica bulk a reduction of $\sim 1.3^\circ$ and $\sim 0.5^\circ$ are recorded for fourfold and threefold rings, respectively.

	D ₁ band	D ₂ band
ω_0 (cm ⁻¹)	495	137.9
θ_0 (degree)	605	127.6

Table IV. Reference data to calculate the inter-tetrahedral angle of the small rings from [31].

Beside the blue-shift, the D₁ and D₂ bands show a broadening, which implies a width increase in the angle θ distribution and in the stress distribution along the rings [32]. Nevertheless, the most evident neutron-induced effect on such bands is an area increase, corresponding to the small ring concentration increase. All the previous studies observed a conspicuous increase of the threefold rings [10,28], whereas the concentration of the four-membered rings generally is more difficult to estimate because of its overlapping with the wider R band. In our case, while the concentration of the threefold rings increases and tends to saturate, regardless of its initial values, which were different in the core and in the cladding, the increase of the fourfold ring concentration seems to occur only in the cladding.

Among all the observed Raman bands, the origin of one remains debated: the one centered at (890.7 ± 1.1) cm⁻¹ with FWHM of (44 ± 6) cm⁻¹. This band has already been observed on neutron-irradiated silica bulk glasses [28] but it has not been clearly assigned yet and two models have been suggested in literature. It could be associated with either:

- a vibrational mode in two-membered rings featuring a threefold-coordinated oxygen, according to *ab initio* calculations [28];
- the vibrational mode of oxygen dangling bonds, which is at (890 ± 10) cm⁻¹ according to low temperature zero phonon line measurements [33].

Indeed, recently, a Raman band peaking at 896 cm⁻¹ with a FWHM of 32 cm⁻¹ was observed in several types of irradiated silica with a high NBOHC concentration (in the order of 10^{18} defects/cm³) and attributed to resonance Raman scattering of such defects, because this band was detectable only when the excitation laser energy was close or matched an NBOHC absorption band [35].

However, our Raman band at 890 cm⁻¹ cannot be attributed to the vibrational mode of oxygen dangling bonds. Indeed, the Raman spectrum of the sample irradiated at the highest fluence was excited with four different excitation laser wavelengths: 325 nm and 633 nm, which fall

within the absorption bands of the NBOHCs, and 442 nm and 785 nm, which do not. As it is clear from the spectra reported in Fig. 11, the Raman band peaking at $\sim 890\text{ cm}^{-1}$ is always present in our irradiated samples regardless of the excitation energy.

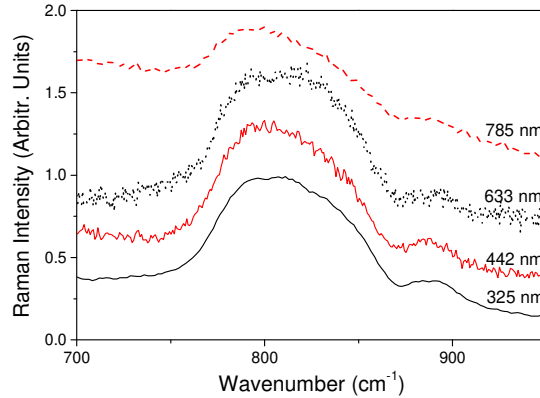


Fig. 11. Zoom of the Raman spectra recorded in the fiber core of the sample irradiated at the highest fluence under excitation with four different laser wavelengths: 325 nm (black continuous line), 442 nm (red continuous line), 633 nm (black dashed line) and 785 nm (red dashed line). The 325 nm and 633 nm excitation lines fall inside the absorption bands of the NBOHC, whereas the other two do not. The spectra were normalized at the band $\sim 800\text{ cm}^{-1}$ and vertically translated. (no color print)

However, the presence of NBOHCs in our sample is not guaranteed. As shown in Fig. 9, a PL band was observed at $\sim 2\text{ eV}$, but its characteristics do not correlate with the ones of a typical PL emitted by NBOHCs, whereas the high concentration of SiOH groups suggests that most of the radiation-induced NBOHCs (by γ -rays and neutrons) interact with H^+ ions; the effect of the high irradiation temperature ($\sim 290^\circ\text{C}$) should also be considered.

These two observations allow us to state that the Raman band at $\sim 890\text{ cm}^{-1}$ observed on the neutron-irradiated silica samples differs from the one at $\sim 896\text{ cm}^{-1}$ associated with the vibrational mode of oxygen dangling bonds. So, the only remaining hypothesis is the vibrational mode in two-membered rings featuring a threefold-coordinated oxygen, proposed by Léon *et al.* on the basis of ab initio calculations [28].

5 CONCLUSION

We used micro-Raman spectroscopy to study the structural changes induced on a pure silica core multimode fiber by a neutron irradiation up to $5 \times 10^{19}\text{ n/cm}^2$, with $\sim 3\text{ }\mu\text{m}$ spatial resolution along the fiber diameter. This technique allows us to state that the densification process is uniform along the whole fiber transverse surface, because the fictive temperature, determined from the R band maximum, does not change with the radial distance from the fiber center. Moreover, it increases by $\sim 500^\circ\text{C}$ compared to the pristine reference. The irradiated sample, whose density increase was of 0.7%, shows the typical densified silica structure: the inter-tetrahedral Si-O-Si angle decrease of $\sim 1^\circ$ for the large rings and $\sim 0.44^\circ$ and $\sim 0.23^\circ$ for the fourfold and threefold rings, respectively. Moreover, an increase of these small ring concentration was detected. However, the three-membered ring concentration reaches a saturation values along the whole fiber diameter, regardless of the initial concentration. Instead, for the four-membered structures, in the core the concentration does not change with the irradiation and slightly increases with the radial distance, whereas it is constant in the pure silica part of the cladding and increases with the neutron fluence of $\sim 20\%$.

The lower densification observed on our neutron-irradiated OF samples at $\sim 290^\circ\text{C}$ is reflected in weaker structural changes, compared to the ones recorded on neutron-irradiated on bulk silica glasses at $\sim 60^\circ\text{C}$ [10]. The cause of such observation could mainly be the irradiation temperature. However, we do not have to forget internal strain related to the optical fiber

drawing is present inside the OF. Additional investigations on more samples are still necessary to provide a more complete picture.

Finally, studies concerning the new Raman band at $\sim 890\text{ cm}^{-1}$ in our neutron exposed sample cannot be associated with the vibrational mode of oxygen dangling bonds. Concerning the PL band at 2.27 eV (546 nm), which characterizes the densified silica samples, both by neutrons or femtosecond laser, its origin remains unknown. We can however state that it is not bleached by the presence of H^+ ions, whereas the NBOHC is.

REFERENCES

- [1] S. Girard, J. Kuhnhenh, A. Gusarov, B. Brichard, M. Van Uffelen, Y. Ouerdane, A. Boukenter, Radiation effects on silica-based optical fibers: recent advances and future challenges, *IEEE Trans. Nucl. Sci.* 60 (2013) 2015. [10.1109/TNS.2012.2235464](https://doi.org/10.1109/TNS.2012.2235464)
- [2] S. Girard, A. Morana, A. Ladaci, T. Robin, L. Mescia, J-J. Bonnefois, M. Boutillier, J. Mekki, A. Paveau, B. Cadier, E. Marin, Y. Ouerdane, A. Boukenter, Recent advances in radiation-hardened fiber-based technologies for space applications, *J. Opt.* 20 (2018) 093001. <https://doi.org/10.1088/2040-8986/aad271>
- [3] L. Remy, G. Cheymol, A. Gusarov, A. Morana, E. Marin, S. Girard, Compaction in optical Fibres and fibre Bragg gratings under nuclear reactor high neutron and gamma fluence, *IEEE Trans. Nucl. Sci.* 63 (2016) 2317–2322. [10.1109/TNS.2016.2570948](https://doi.org/10.1109/TNS.2016.2570948)
- [4] G. Cheymol, L. Remy, A. Gusarov, D. Kinet, P. Mégret, G. Laffont, T. Blanchet, A. Morana, E. Marin, S. Girard, Study of Fiber Bragg grating samples exposed to high fast neutron fluences, *IEEE Trans. Nucl. Sci.* 65 (2018) 2494–2501. [10.1109/TNS.2018.2820505](https://doi.org/10.1109/TNS.2018.2820505)
- [5] G. Buscarino, S. Agnello, F.M. Gelardi, R. Boscaino, Polyamorphic transformation induced by electron irradiation in a-SiO₂ glass, *Phys. Rev. B* 80 (2009) 094202. <https://doi.org/10.1103/PhysRevB.80.094202>
- [6] C. Martinet, V. Martinez, C. Coussa, B. Champagnon, M. Tomozawa, Radial distribution of the fictive temperature in pure silica optical fibers by micro-Raman spectroscopy, *J. Appl. Phys.* 103 (2008) 083506. <https://doi.org/10.1063/1.2905321>
- [7] W. Primak, R. Kampwirth, The Radiation Compaction of Vitreous Silica, *J. Appl. Phys.* 39 (1968) 5651. <https://doi.org/10.1063/1.1656029>
- [8] W. Primak, Fast-Neutron-Induced Changes in Quartz and Vitreous Silica, *Phys. Rev.* 110 (1958) 1240. <https://doi.org/10.1103/PhysRev.110.1240>
- [9] E. Dooryhée, J. P. Duraud, R. A. B. Devine, in *Structure and Imperfections in Amorphous and Crystalline Silicon Dioxide*, (Eds: R. A. B. Devine, J. P. Duraud, E. Dooryhée), Wiley, New York (2000).
- [10] J. B. Bates, R. W. Hendricks, L. B. Shaffer, Neutron irradiation effects and structure of noncrystalline SiO₂, *J. Chem. Phys.* 61 (1974) 4163. <https://doi.org/10.1063/1.1681714>
- [11] C. M. Petrie, A. Birri, T. E. Blue, High-dose temperature-dependent neutron irradiation effects on the optical transmission and dimensional stability of amorphous fused silica, *J. Non-Cryst. Solids* 525 (2019) 119668.
- [12] G. Cheymol, A. Gusarov, S. Gaillot, C. Destouches, N. Caron, Dimensional Measurements Under High Radiation With Optical Fibre Sensors Based on White Light Interferometry - Report on Irradiation Tests, *IEEE Trans. Nucl. Sci.* 61 (2014) 2075-2081. <https://doi.org/10.1109/TNS.2014.2321026>

- [13] S. Girard, A. Alessi, N. Richard, L. Martin-Samos, V. De Michele, L. Giacomazzi, S. Agnello, D. Di Francesca, A. Morana, B. Winkler, I. Reghioua, P. Paillet, M. Cannas, T. Robin, A. Boukenter, Y. Ouerdane, Overview of radiation induced point defects in silica-based optical fibers, *Review of Physics* 4 (2019) 100032. <https://doi.org/10.1016/j.revip.2019.100032>
- [14] N. Shimodaira, K. Saito, E. H. Sekiya, A. J. Ikushima, Microscopic structural changes of SiO₂ glasses as a function of temperature investigated by in situ Raman spectroscopy, *Phys. Rev. B* 73 (2006) 214206. <https://doi.org/10.1103/PhysRevB.73.214206>
- [15] G. S. Henderson, D. R. Neuville, B. Cochain, L. Cormier, The structure of GeO₂–SiO₂ glasses and melts: A Raman spectroscopy study, *J. Non-Cryst. Solids* 355 (2009), 468-474. <https://doi.org/10.1016/j.jnoncrysol.2009.01.024>
- [16] J. Stone, G. E. Walrafen, Overtone vibrations of OH groups in fused silica optical fibers, *J. Chem. Phys.* 76 (1982) 1712. <https://doi.org/10.1063/1.443210>
- [17] G.H.A.M. Van Der Steen, H. Van den Boom, Raman spectroscopic study of hydrogen-containing vitreous silica, *J. Non-Cryst. Solids* 23 (1977) 279-286. [https://doi.org/10.1016/0022-3093\(77\)90010-2](https://doi.org/10.1016/0022-3093(77)90010-2)
- [18] L. Skuja, Optically active oxygen-deficiency-related centers in amorphous silicon dioxide, *J. Non-Cryst. Solids* 239 (1998) 16-48.
- [19] A. Morana, S. Girard, M. Cannas, E. Marin, C. Marcandella, P. Paillet, J. Périssé, J.-R. Macé, R. Boscaino, B. Nacir, A. Boukenter, Y. Ouerdane, *Opt. Mater. Express* **2015**, 5, 898.
- [20] L. Skuja, T. Suzuki, K. Tanimura, Site-selective laser-spectroscopy studies of the intrinsic 1.9-eV luminescence center in glassy SiO₂, *Phys. Rev. B* 52 (1995) 15208. <https://doi.org/10.1103/PhysRevB.52.15208>
- [21] P. Martín, M. León, A. Ibarra, Photoluminescence in neutron irradiated fused silica, *Phys. Stat. Sol. C* 2 (2005) 624. <https://doi.org/10.1002/pssc.200460250>
- [22] M. Royon, E. Marin, S. Girard, A. Boukenter, Y. Ouerdane, R. Stoian, X-ray preconditioning for enhancing refractive index contrast in femtosecond laser photoinscription of embedded waveguides in pure silica, *Opt. Mater. Express* 9 (2019) 65-74. <https://doi.org/10.1364/OME.9.000065>
- [23] R. H. Stolen, J. T. Krause, C. R. Kurkjian, Raman scattering and far infra-red absorption in neutron compacted silica, *Discuss. Faraday Soc.* 50 (1970) 103-107. <https://doi.org/10.1039/DF9705000103>
- [24] K. Nordlund, A. E. Sand, F. Granberg, S. J. Zinkle, R. Stoller, R. S. Averback, T. Suzudo, L. Malerba, F. Banhart, W. J. Weber, F. Willaime, S. Dudarev, D. Simeone, Primary Radiation Damage in Materials, NEA/NSC/DOC 9 (2015).
- [25] R. G. Palmer, Models for Slow Relaxation in Glassy Systems, *Cooperative Dynamics in Complex Physical Systems*, (Ed: H. Takayama), Springer, Berlin, (1989) 118-127 .
- [26] M. Lancry, E. Régnier, B. Poumellec, Fictive Temperature in Silica-Based Glasses and its Application to Optical Fibre Manufacturing, *Prog. Mater. Sci.* 57 (2012) 63-94. [10.1016/j.pmatsci.2011.05.002](https://doi.org/10.1016/j.pmatsci.2011.05.002)
- [27] A. J. Ikushima, T. Fujiwara, K. Saito, Silica glass: A material for photonics, *J. Appl. Phys.* 88 (2000) 1201. <https://doi.org/10.1063/1.373805>
- [28] M. León, L. Giacomazzi, S. Girard, N. Richard, P. Martín, L. Martín-Samos, A. Ibarra, A. Boukenter, Y. Ouerdane, Neutron Irradiation Effects on the Structural Properties of KU1,

- KS-4V and I301 Silica Glasses, *IEEE Trans. Nucl. Sci.* 61 (2014) 1522-1530. 10.1109/TNS.2013.2294033
- [29] J. E. Shelby, Density of vitreous silica, *J. Non-Cryst. Solids* 349 (2004) 331-336. <https://doi.org/10.1016/j.jnoncrysol.2004.08.206>
- [30] P. N. Sen, M. F. Thorpe, Phonons in AX₂ glasses: From molecular to band-like modes, *Phys. Rev. B* 15 (1977) 4030. <https://doi.org/10.1103/PhysRevB.15.4030>
- [31] F. L. Galeener, Band limits and the vibrational spectra of tetrahedral glasses, *Phys. Rev. B* 19 (1979) 4292. <https://doi.org/10.1103/PhysRevB.19.4292>
- [32] B. Hehlen, Inter-tetrahedra bond angle of permanently densified silicas extracted from their Raman spectra, *J. Phys.: Condens. Matter* 22 (2010) 025401. 10.1088/0953-8984/22/2/025401
- [33] J. Burgin, C. Guillon, P. Langot, F. Vallée, B. Hehlen, M. Foret, Vibrational modes and local order in permanently densified silica glasses: Femtosecond and Raman spectroscopy study, *Phys. Rev. B* 78 (2008) 184203. <https://doi.org/10.1103/PhysRevB.78.184203>
- [34] L. Vaccaro, M. Cannas, R. Boscaino, Luminescence features of nonbridging oxygen hole centres in silica probed by site-selective excitation with tunable laser, *Solid State Commun.* 146 (2008) 148-151. <https://doi.org/10.1016/j.ssc.2008.02.001>
- [35] D. Di Francesca, A. Boukenter, S. Agnello, A. Alessi, S. Girard, M. Cannas, Y. Ouerdane, Resonance Raman of oxygen dangling bonds in amorphous silicon dioxide, *J. Raman Spectrosc.* 48 (2016) 230-234. <https://doi.org/10.1002/jrs.5006>